

End-to-End Learning of Multi-category 3D Pose and Shape Estimation

Yigit Baran Can¹ Alexander Liniger¹ Danda Pani Paudel¹ Luc Van Gool^{1,2}

¹Computer Vision Lab, ETH Zurich ²VISICS, ESAT/PSI, KU Leuven

{yigit.can, alex.liniger, paudel, vangool}@vision.ee.ethz.ch

Abstract

In this paper, we study the representation of the shape and pose of objects using their keypoints. Therefore, we propose an end-to-end method that simultaneously detects 2D keypoints from an image and lifts them to 3D. The proposed method learns both 2D detection and 3D lifting only from 2D keypoints annotations. In this regard, a novel method that explicitly disentangles the pose and 3D shape by means of augmentation-based cyclic self-supervision is proposed, for the first time. In addition of being end-to-end in image to 3D learning, our method also handles objects from multiple categories using a single neural network. We use a Transformer-based architecture to detect the keypoints, as well as to summarize the visual context of the image. This visual context information is then used while lifting the keypoints to 3D, so as to allow the context-based reasoning for better performance. While lifting, our method learns a small set of basis shapes and their sparse non-negative coefficients to represent the 3D shape in canonical frame. Our method can handle occlusions as well as wide variety of object classes. Our experiments on three benchmarks demonstrate that our method performs better than the state-of-the-art. Our source code will be made publicly available.

1. Introduction

Keypoint-based shape and pose representation is attractive because of its simplicity and ease of handling. Example applications include 3D reconstruction [8, 28, 38], registration [17, 24, 25, 50], and human body pose analysis [3, 5, 27, 37], recognition [13, 35], and generation [42, 51]. The keypoints are often detected as 2D image coordinates due to the ease of the corresponding annotation. Yet, this often does not suffice for the subsequent geometric reasoning tasks. In fact, in many applications (e.g. as augmented reality), both 3D shape and pose are required [45].

It therefore stands to reason that keypoints should be estimated in 3D, similar to [40, 41, 45, 53]. Such solutions however, come with one or both of the two pitfalls: (i) need of 3D keypoints, pose, or multiple views for supervi-

Method	End-to-end	Multi-class	Single Image	No Test time opt
Park et al. [33]				
Kong et al. [20]			✓	✓
Wang et al. [46]		✓	✓	
Zeng et al. [52]			✓	✓
Novotny et al. [28]		✓	✓	✓
Ours	✓	✓	✓	✓

Table 1. **Our approach in relation to the existing works.**

sion; (ii) the lack of direct pose reasoning with respect to a canonical frame. In this regard, learning based methods can provide both 3D keypoints and pose merely from a single image, making them suitable for a very wide range of applications from scene understanding [11] to augmented reality [26]. Alternatively, template-based single view methods [36, 49] may also be used to obtain 3D keypoints and pose from 2D keypoints. However, template based methods, beside requiring templates, are known to be sensitive to self-occlusions [9]. Therefore, we adopt a learning based method for single view inference of both 3D keypoints and pose of objects.

In this paper, we consider that only one image per object is available both during training and inference. Such assumption allows us to learn from diverse datasets, such as internet image collections, potentially offering us a high generalization ability. For better scalability, we also assume that only minimalistic supervision in the form of 2D keypoints and objects' categories are available. In essence, we wish to learn the 3D keypoints and pose of objects from an image collection of multiple categories, where not even multi-view images of the same object are available.

Existing methods that learn 3D shape and pose from an image collection by object categories are also known as deep non-rigid structure-from-motion (NrSfM) due to their underlying assumption. The method proposed in this paper also belongs to the same class, which can be divided

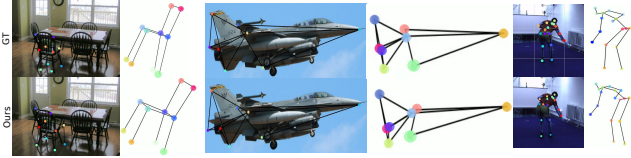


Figure 1. Our method can provide accurate 3D estimations for a wide range of categories, directly from a single image. The 2D keypoints are detected and used in conjunction with an image based feature vector to produce 3D estimates.

into single [20, 33, 46, 52] and multi-category [28] methods. Multi-category methods are strikingly interesting due to two main reasons: (i) computational: one single neural network can infer shapes and poses for objects from different categories; (ii) relational: possibility of establishing/exploiting relationships across categories. The latter does not only let us measure the cross-category similarity but may also have better generalizability.

In the context of multi-category methods, we introduce three major improvements in the form of:

- an end-to-end learning framework directly from images;
- sparse non-negative combination of shape basis;
- the explicit 3D pose and shape disentanglement via an augmentation-based cyclic consistency for supervision.

End-to-end learning: Most existing methods [20, 28, 33, 46, 52] operate in two stages; 2D keypoints extraction followed by 3D shape and pose estimation. These two stages are often performed independently. We argue that these two stages are dependent therefore can mutually benefit from each other. Thus, 2D keypoints can be extracted while being suitable for the down-streaming task of 3D reasoning. In particular, we extract the visual context information along with the 2D keypoints from the keypoint extraction network. Later, both visual context and 2D keypoints are provided to the network that lifts 2D keypoints to 3D. Our experiments clearly demonstrate the benefit of visual context information during 3D pose and shape recovery.

Non-negative shape coefficients: We model 3D shape using a dictionary learning approach, similar to [28], where the shape basis for the union of categories are learned. The instance-wise shape is then recovered with the help of the shape basis coefficients. In this process, only non-negative coefficients are considered. Intuitively, the non-negative shape coefficients allow us to perform the interpolation and the scaling of the learned shape basis. The subtraction between shape basis, although algebraically non problematic, are geometrically less meaningful. Non-negative shape coefficients encourage the shape basis to be geometrically more meaningful, leading to better performance.

Augmentation-based pose and shape disentanglement: During the recovery of shape basis, by factoring 2D measurements into shape and the pose, the pose aspect may largely influence the shape basis, which is not desired [23].

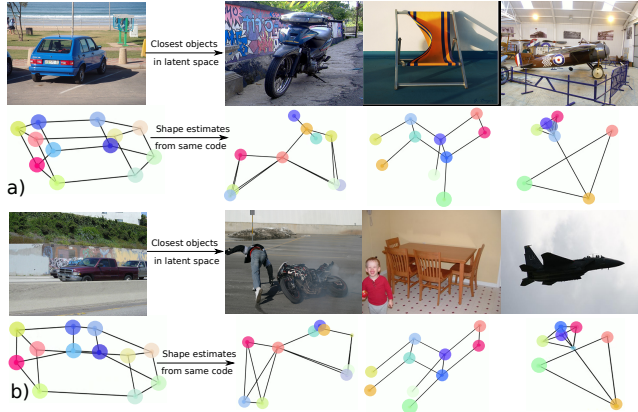


Figure 2. Our method maps all objects into a category-invariant single latent space. This lets the method learn cross-categorical geometric relationships. Here we show two car samples from the validation set in (a) and (b). The images are the per category closest samples in the latent space. The 3D reconstructions are from the latent code of the corresponding car mapped into different categories. Thus 3D shapes are not of the images but rather decoding of the latent codes of the cars. It can be seen that elongation (height/width ratio) is translated across categories.

In this context, [28] refers to shape disentanglement as “shape transversality”, which is done implicitly by undoing random rotations of the estimated shape by an auxiliary neural network. Similarly, a rigidity-based pairwise contrastive loss is proposed in [52] to handle the disentanglement problem implicitly. On the other hand, the methods in [31, 33, 46] use a Procrustean-based approach. The latter approaches do not predict the motion, and rather compute the pose between input and 3D prediction in the canonical frame using orthographic n-point (OnP) solvers [39]. Instead of using the OnP solvers, we simulate multiple instances of the pose by random rotations and perform self-supervision from the viewpoint of data augmentation. In particular, we rotate the generated shape, followed by their 2D projection. The projected 2D keypoints are fed back to the network to recover pose agnostic shape parameters. In other words, our disentanglement explicitly exploits the following fact: the shape coefficients must be the same for keypoints that differ only by poses. This allows us to explore the space of poses that may not be available in the data, making our method more robust to pose variations.

The major contributions of our work can be summarized as:

- End-to-end reconstructing of 3D shape and pose in a multiple category setup, using a single neural network.
- We propose to use non-negative shape coefficients and an augmentation-based self-supervised pose and shape disentanglement method.
- Our method achieves state-of-the-art results in the multi-category setting, with significant improvement.

2. Related Work

The task of lifting 2D keypoints of deformable objects to 3D from a single image has been mostly studied in the context of NrSfM. In NrSfM, the task is recovering the poses and viewpoints from multiple observations in time of an object [1]. Significant research has been carried out in NrSfM to improve the performance through sparse dictionary learning [19, 54], low-rank constraints [10], union of local subspaces [56], diffeomorphism [30] and coarse-to-fine low rank reconstruction [2]. It is possible to use NrSfM frameworks to build category specific models that can learn to estimate pose and viewpoint from a single image by treating the images of the same category as observations of a single object deformed at different time steps [7, 20, 21].

Obtaining the 3D structure of an object given only a single image has been studied sparsely. In [16] instance, segmentation datasets were utilized to train a model that outputs 3D mesh reconstructions given an image. Correspondences between 2D-3D keypoints were also used to improve results [18]. While some recent methods can estimate the viewpoint and non-rigid meshes, these methods work on objects with limited diversity, such as faces [15, 34, 48].

The closest line of work to ours involves building a single model for a diverse set of input classes. C3DPO [29] proposed to learn the factorization of the object deformation and viewpoint change. They propose to enforce the transversal property through a separate canonicalization network that undoes rotation applied on a canonical shape. Park et al. proposed using Procrustean regression [32] to determine unique motions and shapes [33]. However, their method cannot handle multiple object categories or occluded keypoints. Moreover, it requires temporal information in the form of sequences. Recently, [46] extended Procrustean formulation with autoencoders and proposed a method that can infer 3D shapes without the need for sequence. However, their method requires a substantially more complex network as well as optimization at test-time. All these methods accept 2D keypoints as input rather than images and tackle the problem of obtaining 3D keypoint locations from a single image using a separate keypoint detector, such as a stacked hourglass network [44].

3. Multi-category from Single View

We extract 3D structures in the form of 3D keypoints, given only an image of some object category. During training, we only have access to the 2D location of keypoints, including the category label. For simplicity, we separate our solution into two parts: category and 2D keypoints extraction from the image and lifting them to 3D. In the following, we will first explain our approach for lifting the given 2D keypoints. We formulate the lifting of 2D keypoints problem in the context of NrSfM.

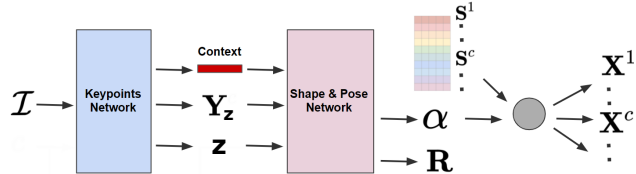


Figure 3. System pipeline. Multi category from single view.

3.1. Preliminaries - NrSfM

Let $\mathbf{Y}_i = [\mathbf{y}_{i1}, \dots, \mathbf{y}_{ik}] \in \mathbb{R}^{2 \times k}$ be a stacked matrix representation of k 2D keypoints from the i^{th} view. We represent the structure of the i^{th} view as $\mathbf{X}_i = \alpha_i^T \mathbf{S}$, using the shape basis $\mathbf{S} \in \mathbb{R}^{d \times 3k}$ and coefficients $\alpha_i \in \mathbb{R}^d$. For simplicity, we assume that the keypoints are centered and normalized, and that the camera follows an orthographic projection model, represented by $\Pi = [\mathbf{I}_{2 \times 2} \ \mathbf{0}]$. Given the camera rotation matrix $\mathbf{R}_i \in \mathbf{SO}(3)$, and the centered, and normalized keypoints, we can write $\mathbf{Y}_i = \Pi \mathbf{R}_i (\mathbb{I}_3 \odot \alpha_i^T \mathbf{S})$, where the operation $\mathbb{I}_3 \odot \mathbf{s}$ reshapes the row vector $\mathbf{s} \in \mathbb{R}^{1 \times 3k}$ to a matrix of the form $\mathbb{I}_3 \odot \mathbf{s} \in \mathbb{R}^{3 \times k}$. The recovery of shape and pose by NrSfM given n views can be written as¹,

$$\min_{\alpha_i, \mathbf{S}, \mathbf{R}_i \in \mathbf{SO}(3)} \sum_{i=1}^n \mathcal{L}(\mathbf{Y}_i, \Pi \mathbf{R}_i (\mathbb{I}_3 \odot \alpha_i^T \mathbf{S})). \quad (1)$$

where $\mathcal{L}(a, b)$ is a norm-based loss of the form $\|a - b\|$.

The above problem is generally ill-posed. Thus, different assumptions regarding α_i and \mathbf{S} are made in the literature. The most common constraints in this regard are, low-rank [8], finite-basis [47], and sparse combination [55]. In this work, we are interested to solve the problem of (1) using a learning based approach. We, however, are further interested in multi-category setting of single view inference.

3.2. Multi-category Formulation

In the context of multi-class NrSfM, our method extracts 3D structures of objects from wide variety of classes. Thus, $(\mathbb{I}_3 \odot \alpha_i^T \mathbf{S}) \in \mathbb{R}^{3 \times k}$, should be able to express 3D structure of objects with different number of keypoints. Let \mathbf{Z} represent the set of object categories and $z_i \in \mathbf{Z}$ be the category of sample i . Let each category $z \in \mathbf{Z}$ be represented by k_z keypoints. Then we set the number of total keypoints $k = \sum_z k_z$. We have a subset selection vector $\zeta_z \in \{0, 1\}^k$ that indicates which dimensions relates to the category z . Then, formula 1 can be rewritten as

$$\min_{\alpha_i, \mathbf{S}, \mathbf{R}_i \in \mathbf{SO}(3)} \sum_{i=1}^n \mathcal{L}(\mathbf{Y}_i \odot \zeta_{z_i}, \Pi \mathbf{R}_i (\alpha_i^T \mathbf{S}) \odot \zeta_{z_i}), \quad (2)$$

where \odot is the broadcasted elementwise multiplication.

In the above formulation, \mathbf{R}_i and α_i are inputs, hence category dependent, while \mathbf{S} is shared among all categories. To formulate the problem as a learning-based approach, let us separate α_i into two composite functions

¹We will omit \mathbb{I}_3 and the transposition of α throughout the rest of the paper for the ease of notation.

$\alpha(\mathbf{Y}) = g(f(\mathbf{Y}))$, with $g(\cdot)$ being an affine function, $g(v) = W_g v + b_g$ with $v \in \mathbb{R}^F$, $W_g \in \mathbb{R}^{D \times F}$, $b_g \in \mathbb{R}^D$. Moreover, let us rewrite \mathbf{R}_i as a function of input y , i.e. $R(y)$. Representing all the parameters with θ , the problem definition becomes

$$\min_{\theta} \sum_i \mathcal{L}(\mathbf{Y} \circ \zeta_{z_i}, \Pi(R(\mathbf{Y})([W_g f(\mathbf{Y}) + b_g] \mathbf{S}) \circ \zeta_{z_i})). \quad (3)$$

In the above formulation, shape basis coefficients α_i are latent codes with the latent space basis vectors W_g and a translation term b_g , which are shared for all categories. Projecting features of objects from different categories into a shared latent space lets the method extract cross-categorical geometric relationships, as shown in Fig. 2. Moreover, it substantially simplifies computations since we do not require a separate network for each class.

3.3. Non-negative Shape Coefficients

Formula 3 is under-determined unless there are additional constraints imposed on the system. The most common constraint is restricting the dimension D of the shape basis coefficients α_n [1, 4]. However, selecting the optimal cardinality requires careful hyperparameter tuning [28, 33].

Since our method extracts 3D structures of objects from a wide variety of classes, the latent space has to accommodate latent codes from wide range of inputs. Considering most objects share some common characteristics, using different manifolds for each class results in failure to utilize cross-class information as well as increasing complexity of the method. On the other hand, the dimensionality of the optimal manifold is different for each class. Therefore, optimally, we would like to automatically select a manifold for each input in a way that maximizes the performance. Note that the optimal manifold selection depends not only on the object class, but we would like the method to discover cross-class rules for manifold assignment.

Given a sample Y_n , let the selected basis vectors among \mathbf{S} be denoted by a binary vector $\mathbb{I}_n \in \{0, 1\}^D$ where $\sum_d \mathbb{I}_n[d] \leq D; \forall n$, with the basis coefficients $\alpha_n \in \mathbb{R}^D$. Then, the representation of Y_n is $\psi_n = (\mathbb{I}_n \circ \alpha_n) \mathbf{S}$.

This representation is difficult to use with neural networks since the basis selection vector \mathbb{I} is binary and non-differentiable. Let us consider the cone $\text{cone}(\mathbf{S})$ that is defined by the basis vectors \mathbf{S} . Then, $\text{cone}(\mathbf{S}) = \sum_d \beta_d S_d, \beta_d \in \mathbb{R}_{\geq 0}$. Thus, it is the space covered by \mathbf{S} when the basis coefficients are non-negative. Let us assume that $\psi_n = (\mathbb{I}_n \circ \alpha_n) \mathbf{S}$, is bounded, i.e. $\exists M \in \mathbb{R}; M > \|\psi_n\|, \forall n$. Then, ψ_n is bounded within a $3K$ dimensional sphere of radius M . Let the axis vector of the cone formed by $\text{cone}(\mathbf{S})$ be b_S . Then $\exists b_S, \|b_S\| > M$, s.t., $\exists \beta; \sum_d \beta_d S_d = \psi_n - b_S; \forall n$. This means, we can translate the sphere that encloses ψ_n in such a way that it is

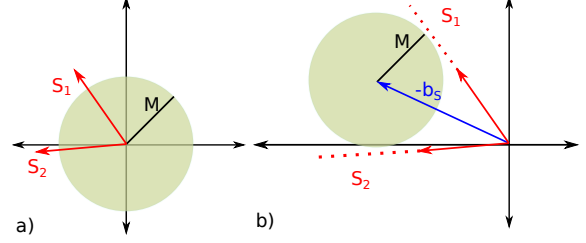


Figure 4. The original shape space is given on the left with basis vectors S_1 and S_2 . We translate the space covering the in-distribution points in the shape space by b_S and limit the coefficients of the basis vectors to non-negative values.

completely covered by the cone of the basis vectors. Rearranging terms, we arrive at the equation $\psi_n = \beta_n \mathbf{S} + b_S$.

This result implies that we can restrict the basis coefficients α_n to $\mathbb{R}^+ \cup \{0\}$ by adding a translation term b_S . With these adjustments, we rewrite $\psi_n = \max[(\alpha_n, \mathbf{0})] \mathbf{S} + b_S$. Plugging it into 3 we get

$$\mathcal{L}(\mathbf{Y} \circ \zeta, \Pi(R(\mathbf{Y})(\text{ReLU}(W_g f(\mathbf{Y}) + b_g) \mathbf{S} + b_S) \circ \zeta)) \quad (4)$$

With Eq. 4, the method learns to adaptively pick the basis vectors to activate, thus selecting the dimensionality of the manifold. The resulting structure is very simple and all the parameters, including the shape basis vectors \mathbf{S} , the coefficient generating function $W_g f(\cdot) + b_g$ and the bias b_S , are learned from the data. The manifold selection rule is embedded in the thresholding operation applied by ReLU. Note that $\psi_n \in \mathbb{R}^{3K}$ is the network's output, i.e. the 3D locations of the keypoints. Thus, in-distribution inputs are expected to produce bounded estimates.

The proposed formulation has the property of being sparse. This encourages the representation of the objects in shape space, i.e. coefficients α to be disentangled. Intuitively, as the number of active (non-zero) coefficients increases, more different combinations of the shape basis vectors \mathbf{S} can arrive at the same solution. By decreasing the active coefficients adaptively, we force a small number of shape coefficients to represent changes from one object to another. Thus each coefficient represents a different major variation. Moreover, the cutoff imposed by ReLU implies that a small change in the coefficients will, likely, not result in any change in the output as long as the coefficient is inactive. This improves the robustness of the overall method.

3.4. Augmented Self-Supervision

Previous works acknowledged the issue of shape and pose entanglement, and addressed it using canonicalization functionality. While [28] learned a function that undoes any rotation on estimated canonical shape, [31, 46] used a Procrustean framework. However, in both settings, the method can produce transversal estimates only on the in-distribution inputs since canonicalization is applied separately on the

output of the 2D-3D lifter network. Thus, the input 2D keypoints can only be augmented by in plane rotations, which hinders the generalizability of the overall method.

We propose a 3D augmentation approach, which only uses the lifter network. The lifter network accepts $\mathbf{Y} = \tilde{\mathbf{R}}\tilde{\mathbf{X}}$ as inputs, with $\tilde{\mathbf{R}} \in \mathbf{SO}(3)$ and $\tilde{\mathbf{X}} \in \Upsilon$ and outputs the shape estimate $\hat{\mathbf{X}} = \alpha(\mathbf{Y})\mathbf{S}$ and pose $\hat{\mathbf{R}} = R(\mathbf{Y})$. Here, Υ is the set of shapes in the true distribution. In this setting, the input \mathbf{Y} covers projections of all rotations of true distribution shapes. However, the training set does not include all the projections of the true distribution shape samples. Since we do not have access to 3D keypoint locations, we cannot directly augment the input samples. However, we can perform augmentations on the estimated 3D keypoints produced by the lifter network. Thus, let $f(\mathbf{Y}) = \alpha(\mathbf{y})\mathbf{S}$ be the 3D output of the lifter network, then, we propose the following cyclic augmented self supervision

$$\mathcal{L}_{\text{cycle}} = \mathcal{L}(f(\Pi\tilde{\mathbf{R}}f(\Pi\tilde{\mathbf{R}}\tilde{\mathbf{X}})), f(\Pi\tilde{\mathbf{R}}\tilde{\mathbf{X}})), \quad (5)$$

where $\tilde{\mathbf{R}} \in \mathbf{SO}(3)$ is any rotation matrix. This loss encourages the lifter network to be transversal in its outputs since any rotation of its shape estimate $\tilde{\mathbf{X}}$ is mapped back to $\tilde{\mathbf{X}}$. Different than [28], our formulation lets the lifter network f to explore all the rotations of the true distribution shapes. Moreover, all the modifications made on f , such as restricting latent space dimensionality and non-negative coefficients, naturally help improve the cycle supervision. In the training we break down the cyclic loss into two losses:

- Camera loss $\mathcal{L}_c = \mathcal{L}(\tilde{\mathbf{R}}, R(\Pi\tilde{\mathbf{R}}f(\mathbf{Y}) \circ \zeta))$
- Shape loss $\mathcal{L}_s = \mathcal{L}(f(\Pi\tilde{\mathbf{R}}f(\mathbf{Y}) \circ \zeta) \circ \zeta, f(\mathbf{Y}) \circ \zeta)$

These losses ensure that the method can estimate the random rotation $\tilde{\mathbf{R}}$ and maintain the same canonical shape. One important benefit of our formulation is that we do not require an additional network to validate the estimated 3D shapes such as discriminators in GAN based approaches [22] or canonicalization networks [28, 46]. Furthermore, by using our augmentation-based approach our network learns to deal with “imperfect” keypoints, which is fundamental when working with estimated 2D keypoints. Note that, by simply rewriting $f(\mathbf{Y}) = \text{ReLU}(\alpha(\mathbf{Y}))\mathbf{S} + b_S$, cyclic supervision can be extended with non-negative coefficients.

4. End-to-End Learning from Images

The image of an object can be used for more than only 2D keypoint extraction. We propose to detect the 2D keypoints from the image and extract a context vector that can be used in conjunction with the 2D keypoints to obtain a better 3D estimation. The detected 2D keypoints and context vector are used by the lifter network, in our end-to-end trainable pipeline.

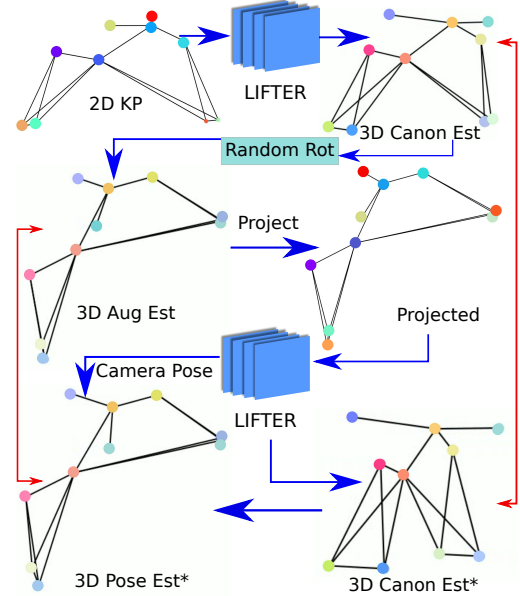


Figure 5. The estimated canonical shape is randomly rotated and projected. The resulting 2D keypoints are fed back to the network. The method should produce the same canonical shape while reproducing the random rotation matrix in the form of camera pose. Blue arrows show process steps while red arrows show loss pairs.

4.1. Keypoints from Images

We require a method that can output the locations of an object category dependent pre-defined set of keypoints. Therefore, the problem at hand naturally extends to object classification. Moreover, in order to fully utilize the image, the keypoint network should produce a context feature representation from the image that can guide the lifter network. Thus, the desired function is $T(\mathcal{I}) = (\mathbf{Y}_z, \mathbf{z}, \rho)$ where \mathcal{I} is the image, \mathbf{Y}_z is the category dependent keypoint locations, \mathbf{z} the category of the object and ρ is the context vector.

We propose to use a DETR-based [6] architecture at the core of function T . Thus, the input image is processed by the backbone (Resnet50 [14]), and the resulting feature map is fed to the transformer. The transformer uses two sets of learned query vectors. The first set is related to keypoints, where each query vector q represents a keypoint. To formalize this, let the maximum number of keypoints among all categories be $\max_z k_z$ be K . Thus, we can extract 2D locations $\delta \in [0, 1]^2$ and the semantics $\omega \in \{0, 1\}^K$ of each keypoint by processing the corresponding query vector using two MLPs. The semantics of a keypoint is category dependent and encoded as a one-hot vector. For example, a given entry in ω can correspond to the front right of a car or the left rear leg of a chair. Entries of ω with indices larger than k_z are zero. The true semantics are denoted by Ω .

To help the lifter network estimate the 3D keypoints, the visual context in the image is important, this is especially

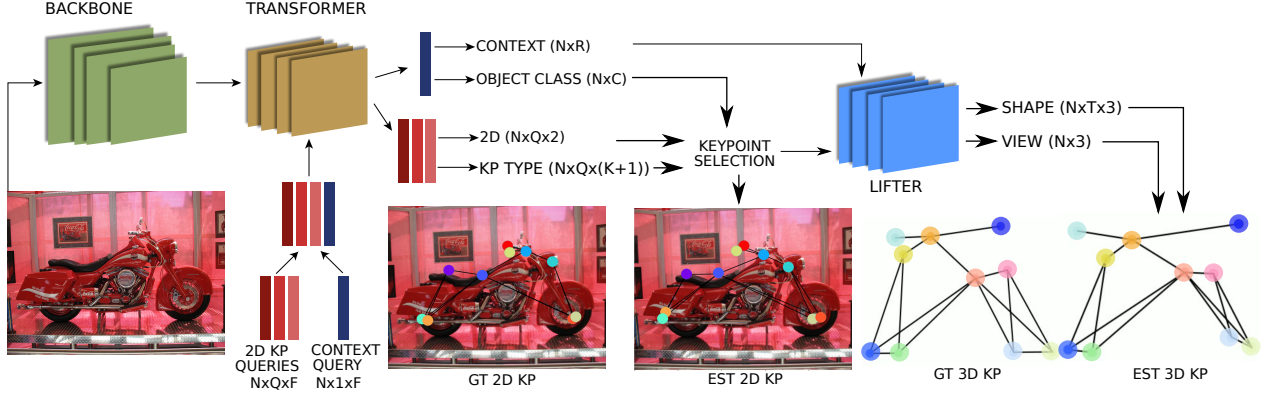


Figure 6. Our method utilizes transformer architecture to extract 2D keypoints, object class and a context vector. The detected keypoints and the context vector are processed by a fully connected neural network to output 3D keypoints and viewpoint from only a single image. The whole end-to-end training only uses 2D keypoint annotations.

true in multi-category examples with large in-category variations. Thus, we use a second set of learned query vectors, which gets processed by the transformer together with the keypoint queries. The output of the transformer for the context query is then processed by two MLPs. The first outputs a N_ρ dimensional context vector and the second \hat{z} the one-hot encoded category probability. The category probability is used in conjunction with the keypoint type estimates to obtain the correct 2D keypoint representation, while the context vector is used by the lifter network together with the 2D keypoint representation, see Fig. 6.

The training of the network has two types of supervision. First, we perform direct supervision of the 2D keypoints and the category-specific outputs ω and c , where we use Hungarian matching to select the supervision targets. Second, by training end-to-end, the keypoint extraction network also receives supervision information via the lifter network, which helps to learn the lifting and keypoint regression jointly. This is also the indirect supervision signal that guides the learning of the context ρ . This end-to-end connection of the lifter and keypoint extraction network is in sharp contrast to existing papers, which focused on either of the two parts. We will show in the results that the combination of the two can give great performance benefits.

4.2. End-to-end Pipeline

Given the end-to-end joint 2D-3D model, the first step in the training loop is Hungarian matching over the keypoint queries and the GT keypoints. For this, the loss to minimize is given by $\mathcal{L}_H = \mathcal{L}_l + \mathcal{L}_k$ where $\mathcal{L}_l = \|y - \delta\|_1$ and $\mathcal{L}_k = \mathcal{L}_{CE}(\Omega, \omega)$. The Hungarian matching output provides the set of query vectors that are one-to-one matched to true keypoints. We reformat selected location estimates $\hat{\delta}$ using the matched semantics $\hat{\omega}$ and the category estimate \hat{z} into the form given in Eq. 2. Let this extracted 2D keypoint representation be \hat{Y} and the true keypoints be \bar{Y} . Adding the category loss of the keypoint network, we arrive at the

following set of losses.

- Location loss $\mathcal{L}_l = \|\bar{Y} - \hat{\delta}\|_1$
- KP Type loss $\mathcal{L}_k = \mathcal{L}_{CE}(\Omega, \hat{\omega})$
- Category loss $\mathcal{L}_b = \mathcal{L}_{CE}(\bar{z}, \hat{z})$
- Reprojection loss $\mathcal{L}_r = \mathcal{L}(\bar{Y} \circ \zeta, \Pi R(\hat{\delta}, \rho) f(\hat{\delta}, \rho) \circ \zeta)$
- Camera loss $\mathcal{L}_c = \mathcal{L}(\bar{\mathbf{R}}, R(\Pi \bar{\mathbf{R}} f(\hat{\delta}, \rho) \circ \zeta))$
- Shape loss $\mathcal{L}_s = \mathcal{L}(f(\Pi \bar{\mathbf{R}} f(\hat{\delta}, \rho) \circ \zeta, \rho) \circ \zeta, f(\hat{\delta}, \rho) \circ \zeta)$

where we use Huber loss for $\mathcal{L}_r, \mathcal{L}_c, \mathcal{L}_s$. For the total loss, the different terms are combined using hyperparameters.

During evaluation, where we cannot use Hungarian matching, we first get the object category estimate \hat{z} . Then, for each keypoint type defined for that category, we take the location of the most likely proposal and convert it into the form given in Eq. 2 to obtain \hat{y} .

5. Experiments

5.1. Datasets

We experiment on the **Synthetic Up3D (S-Up3D)**, **PASCAL3D+** and **Human3.6M** datasets. For all the datasets, we use the pre-processed versions of [28].

5.2. Baselines

There are only few NrSfM methods that can handle as diverse settings as our method. We compare against C3DPO [29] and PAUL [46] in all datasets since they can produce accurate estimates in a wide range of datasets and settings. We also report results of EMSfM [43] and GbNrSfM [12] on the S-Up3D and PASCAL3D datasets. We compare against [33] and [22] only in the Human3.6M dataset since they cannot handle occlusions or multiple object categories. In PASCAL3D, we also compare against CMR [16]. We report results of our lifter network without (Ours-base) and with cycle-supervision (Ours).

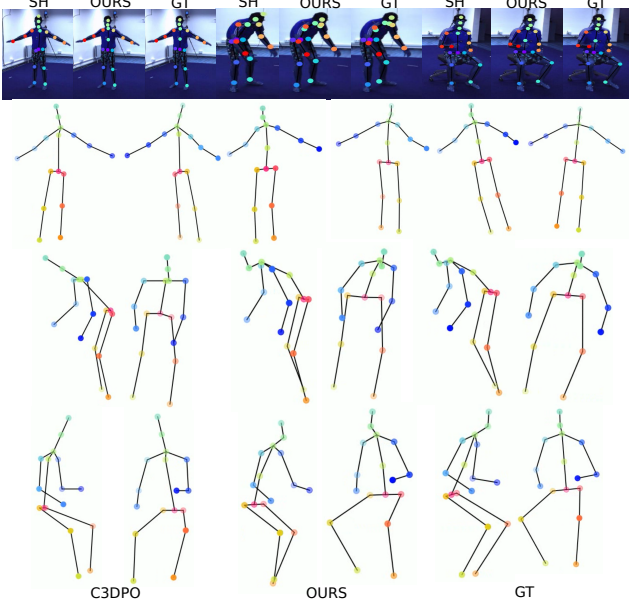


Figure 7. Visual results on the Human3.6M dataset. 2D keypoint estimates of ours, HRNet (SH) from [28] and GT, plus 3D structures from 2 angles for C3DPO, ours and GT.

To validate the end-to-end pipeline, we report results with three settings: 1) Lifter and transformer are trained separately without context vector (Ours/TR); 2) Lifter and transformer are trained end-to-end without context vector (Ours w/o Context); 3) The proposed end-to-end training with context vector (Ours). Moreover, we also experiment with using the stacked hourglass network [44] to extract 2D keypoints on the Pascal3D and Human3.6M datasets.

5.3. Evaluation protocol

Following [29], we report absolute mean per joint position error $MPJPE(X, Y) = \sum_{k=1}^K \|X_k - Y_k\| / K$ as well as $Stress(X, Y) = \sum_{i < j} (\|X_i - X_j\| - \|Y_i - Y_j\|)_+ / (K(K-1))$, where we center both the estimates and ground truth at zero mean. To calculate MPJPE, we apply flip the depth dimension and calculate MPJPE for both cases, keeping the best as our result. This is done to resolve the depth ambiguity problem where the network can assign the depth negative or positive direction.

5.4. Implementation

For experiments with GT keypoints, where only our lifter network is used, we only use visible keypoints as inputs. We mask out the invisible points and concatenate the visibility mask along with the input keypoints. Our keypoint extraction network estimates all keypoints, thus, the jointly trained lifter network also uses all the extracted keypoints. In order to provide a fair comparison, we use the exact same architecture and data pre-processing as [29] for our lifter.

In our experiments with GT keypoints, we deploy two

training schemes. In the first one, we calculate training loss only over the visible keypoints and in the second we calculate the loss over all the keypoints. Note that in both settings, the input of the network is only the visible points and the output is all the keypoints. We refer to the setting with loss calculation over all keypoints with suffix **A**.

6. Results

In order to show the performance of individual components, we separate the results into two parts: using GT 2D keypoints and estimating the keypoints from the image.

6.1. Results with GT Keypoints

We present our results for the lifter network when the GT keypoints are used in Table 2. Our method outperforms all methods that do not perform test-time optimization with using only visible keypoints in training. Moreover, Ours-A outperforms all methods in the Pascal3D dataset where our method’s multi-class focus is shown best. We also outperform all methods in S-Up3D dataset. Comparing C3DPO-base and Ours-base, the clear boost the non-negative coefficients provide can be seen. The proposed cyclic self-supervision also makes a significant contribution. It can be seen that our method is only slightly worse than the Procrustean network [31] in the Human3.6M dataset although they use sequences for training as well as test-time optimization.

Method	Pascal3D		Human3.6M		S-Up3D	
	MPJPE	Stress	MPJPE	Stress	MPJPE	Stress
EM-SfM [43]	131.0	116.8	-	-	0.107	0.061
GbNrSfM [12]	184.6	111.3	-	-	0.093	0.062
PoseGAN [22]	-	-	130.9	51.8	-	-
Proc †* [33]	-	-	86.4	-	-	-
PAUL † [46]	30.9	-	88.3	-	0.058	-
C3DPO-base	53.5	46.8	135.2	56.9	0.160	0.105
C3DPO [28]	38.0	32.6	101.8	43.5	0.068	0.040
Ours-base	40.7	34.1	101.9	46.0	0.080	0.059
Ours	35.4	30.6	92.8	42.6	0.063	0.038
Ours-A	29.5	26.6	92.8	42.6	0.057	0.035

Table 2. Results on Pascal3D, Human3.6M and S-Up3D datasets with GT keypoints. †: Method uses test time optimization. *: Method requires temporal sequences for training.

6.2. Results with Estimated Keypoints

The results with estimated keypoints are given in Table 3. In both datasets our method significantly outperforms the competitors. We see that the performance boost mainly comes from the proposed joint training and the context vector. Especially test-time optimization methods, even when competitive with GT keypoints, suffer considerably using

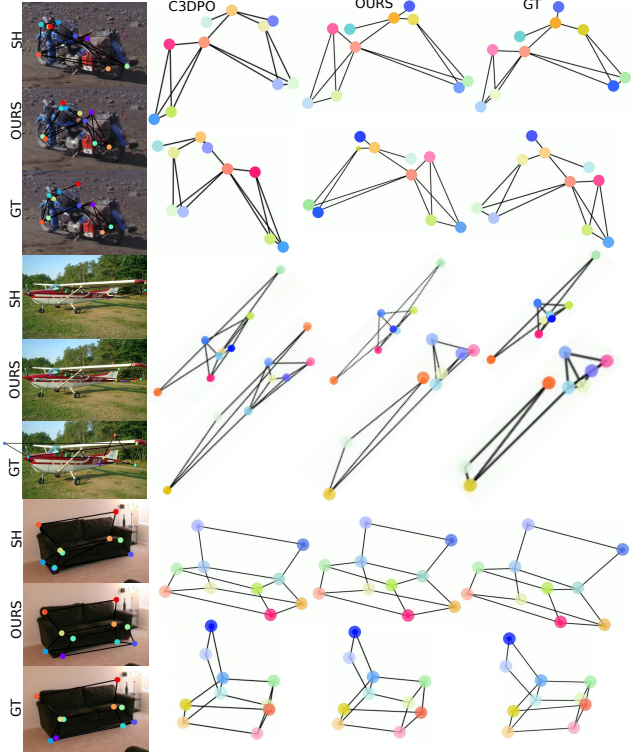


Figure 8. Visual results on the Pascal3D dataset. 2D keypoint estimates of ours, HRNet (SH) from [28] an GT, plus 3D structures from 2 angles for C3DPO, ours and GT.

estimated keypoints, visible in the Human3.6M results. For the Pascal dataset, neither PAUL [46] nor Procrustean network [31] even report numbers.

Method	Pascal3D		Human3.6M	
	MPJPE	Stress	MPJPE	Stress
CMR/SH [16]	74.4	53.7	-	-
C3DPO/SH [28]	57.4	41.4	145.0	84.7
Proc-SH [†] * [33]	-	-	124.5	-
PAUL-SH [†] [46]	-	-	132.5	-
Ours/SH	56.1	39.0	140.7	80.9
Ours/TR	61.3	47.9	114.0	58.8
Ours w/o Cont	57.6	42.9	113.8	56.7
Ours	48.7	35.0	107.7	55.4

Table 3. Results on Pascal3D and Human3.6M datasets. [†]: Method uses test time optimization. *: Method requires temporal sequences for training. SH is pre-trained on additional datasets.

6.3. Multi-Class Ablation

To show the benefits of a multi-category setting, we truncate Pascal3D to a one-class dataset and train our architecture. We repeat this for three different classes. The results, given in Table 4, show that the multi-class trained network significantly outperforms the single category counterparts.

The visual examinations shown in Fig. 2 already demonstrated that the latent space of the multi-category network expresses cross-categorical geometric variations.

Method	Car		Airplane		Chair	
	MJPE	Stress	MJPE	Stress	MJPE	Stress
Car	94.0	65.7	-	-	-	-
Airplane	-	-	26.1	18.6	-	-
Chair	-	-	-	-	15.7	9.5
All	32.8	27.0	17.1	12.4	10.7	7.0

Table 4. Results from the same network architecture when trained on single category vs all.

6.4. Disentanglement

In order to evaluate the effect of the proposed modifications on the latent space, we measured mutual coherence of the latent space basis vectors W_g . The linear combinations of these vectors create the latent code that is then decoded into the 3D keypoints via S . Thus, the mutual coherence of the latent basis vectors provides a measure of disentanglement. Table 5 shows that sparse non-negative coefficients encourage latent basis vectors to be less correlated. Moreover, cyclic self-supervision preserves this latent structure.

Method	S-Up-3D	Pascal3D	Human3.6M
C3DPO	0.89	0.84	0.44
Ours-base (ReLU)	0.36	0.38	0.24
Ours-cycle (ReLU)	0.36	0.39	0.19

Table 5. Mutual coherence of the latent space basis vectors W_g for different methods on all datasets.

7. Conclusion

We study the problem of estimating 3D pose and shape from a single image for objects of multiple categories, in an end-to-end manner. Our learning framework relies only on 2D annotations of keypoints for supervision, and exploits the relationships between keypoints within and across categories. From our experiments two major conclusions can be drawn: (a) multi-category learning is not only beneficial for computational reasons but also offers performance boost; (b) the end-to-end learning process improves the performance of the downstream task. Our method is first of its kind, which outperforms all the compared methods in estimating 3D shape and pose directly from images, on three benchmark datasets.

Limitations. We have observed unstable training in cyclic-self supervision due to batch norm. Batch norm is known to be problematic in recursive use. Thus we first pre-train the network without cycle and fine tune with cyclic loss by freezing batch norm layers to decrease instability.

References

- [1] Ijaz Akhter, Yaser Sheikh, Sohaib Khan, and Takeo Kanade. Trajectory space: A dual representation for nonrigid structure from motion. *IEEE Trans. Pattern Anal. Mach. Intell.*, 33(7):1442–1456, 2011. [3](#), [4](#)
- [2] Adrien Bartoli, Vincent Gay-Bellile, Umberto Castellani, Julien Peyras, Søren I. Olsen, and Patrick Sayd. Coarse-to-fine low-rank structure-from-motion. In *2008 IEEE Computer Society Conference on Computer Vision and Pattern Recognition (CVPR 2008), 24-26 June 2008, Anchorage, Alaska, USA*. IEEE Computer Society, 2008. [3](#)
- [3] Federica Bogo, Angjoo Kanazawa, Christoph Lassner, Peter Gehler, Javier Romero, and Michael J Black. Keep it smpl: Automatic estimation of 3d human pose and shape from a single image. In *European Conference on Computer Vision*, pages 561–578. Springer, 2016. [1](#)
- [4] Christoph Bregler, Aaron Hertzmann, and Henning Biermann. Recovering non-rigid 3d shape from image streams. In *2000 Conference on Computer Vision and Pattern Recognition (CVPR 2000), 13-15 June 2000, Hilton Head, SC, USA*, pages 2690–2696. IEEE Computer Society, 2000. [4](#)
- [5] Zhe Cao, Tomas Simon, Shih-En Wei, and Yaser Sheikh. Realtime multi-person 2d pose estimation using part affinity fields. In *Proceedings of the IEEE Conference on Computer Vision and Pattern Recognition*, pages 7291–7299, 2017. [1](#)
- [6] Nicolas Carion, Francisco Massa, Gabriel Synnaeve, Nicolas Usunier, Alexander Kirillov, and Sergey Zagoruyko. End-to-end object detection with transformers. In Andrea Vedaldi, Horst Bischof, Thomas Brox, and Jan-Michael Frahm, editors, *Computer Vision - ECCV 2020 - 16th European Conference, Glasgow, UK, August 23-28, 2020, Proceedings, Part I*, volume 12346 of *Lecture Notes in Computer Science*, pages 213–229. Springer, 2020. [5](#)
- [7] Geonho Cha, Minsik Lee, and Songhwai Oh. Unsupervised 3d reconstruction networks. In *2019 IEEE/CVF International Conference on Computer Vision, ICCV 2019, Seoul, Korea (South), October 27 - November 2, 2019*, pages 3848–3857. IEEE, 2019. [3](#)
- [8] Y. Dai, H. Li, and M. He. A simple prior-free method for non-rigid structure-from-motion factorization. In *CVPR*, 2012. [1](#), [3](#)
- [9] Zheng Dang, Fei Wang, and Mathieu Salzmann. 3d registration for self-occluded objects in context. *arXiv preprint arXiv:2011.11260*, 2020. [1](#)
- [10] Ingrid Daubechies, Michel Defrise, and Christine De Mol. An iterative thresholding algorithm for linear inverse problems with a sparsity constraint. *Communications on Pure and Applied Mathematics: A Journal Issued by the Courant Institute of Mathematical Sciences*, 57(11):1413–1457, 2004. [3](#)
- [11] Clara Fernandez-Labrador. *Indoor Scene Understanding using Non-Conventional Cameras*. PhD thesis, Université de Bourgogne Franche-Comté (COMUE)(UBFC), FRA.; Universidad . . . , 2020. [1](#)
- [12] Katerina Fragkiadaki, Marta Salas, Pablo Andrés Arbeláez, and Jitendra Malik. Grouping-based low-rank trajectory completion and 3d reconstruction. In Zoubin Ghahramani, Max Welling, Corinna Cortes, Neil D. Lawrence, and Kilian Q. Weinberger, editors, *Advances in Neural Information Processing Systems 27: Annual Conference on Neural Information Processing Systems 2014, December 8-13 2014, Montreal, Quebec, Canada*, pages 55–63, 2014. [6](#), [7](#)
- [13] Kaifeng He, Georgia Gkioxari, Piotr Dollár, and Ross Girshick. Mask r-cnn. In *Proceedings of the IEEE international conference on computer vision*, pages 2961–2969, 2017. [1](#)
- [14] Kaifeng He, Xiangyu Zhang, Shaoqing Ren, and Jian Sun. Deep residual learning for image recognition. In *2016 IEEE Conference on Computer Vision and Pattern Recognition, CVPR 2016, Las Vegas, NV, USA, June 27-30, 2016*, pages 770–778. IEEE Computer Society, 2016. [5](#)
- [15] Simon Jenni and Paolo Favaro. Self-supervised multi-view synchronization learning for 3d pose estimation. In Hiroshi Ishikawa, Cheng-Lin Liu, Tomás Pajdla, and Jianbo Shi, editors, *Computer Vision - ACCV 2020 - 15th Asian Conference on Computer Vision, Kyoto, Japan, November 30 - December 4, 2020, Revised Selected Papers, Part V*, volume 12626 of *Lecture Notes in Computer Science*, pages 170–187. Springer, 2020. [3](#)
- [16] Angjoo Kanazawa, Shubham Tulsiani, Alexei A. Efros, and Jitendra Malik. Learning category-specific mesh reconstruction from image collections. In Vittorio Ferrari, Martial Hebert, Cristian Sminchisescu, and Yair Weiss, editors, *Computer Vision - ECCV 2018 - 15th European Conference, Munich, Germany, September 8-14, 2018, Proceedings, Part XV*, volume 11219 of *Lecture Notes in Computer Science*, pages 386–402. Springer, 2018. [3](#), [6](#), [8](#)
- [17] Laurent Kneip, Hongdong Li, and Yongduek Seo. Upnp: An optimal o(n) solution to the absolute pose problem with universal applicability. In David Fleet, Tomas Pajdla, Bernt Schiele, and Tinne Tuytelaars, editors, *Computer Vision - ECCV 2014: 13th European Conference, Zurich, Switzerland, September 6-12, 2014, Proceedings, Part I*, 2014. [1](#)
- [18] Filippos Kokkinos and Iasonas Kokkinos. To the point: Correspondence-driven monocular 3d category reconstruction. *CoRR*, abs/2106.05662, 2021. [3](#)
- [19] Chen Kong and Simon Lucey. Prior-less compressible structure from motion. In *2016 IEEE Conference on Computer Vision and Pattern Recognition, CVPR 2016, Las Vegas, NV, USA, June 27-30, 2016*, pages 4123–4131. IEEE Computer Society, 2016. [3](#)
- [20] Chen Kong and Simon Lucey. Deep non-rigid structure from motion. In *2019 IEEE/CVF International Conference on Computer Vision, ICCV 2019, Seoul, Korea (South), October 27 - November 2, 2019*, pages 1558–1567. IEEE, 2019. [1](#), [2](#), [3](#)
- [21] Chen Kong, Rui Zhu, Hamed Kiani, and Simon Lucey. Structure from category: A generic and prior-less approach. In *Fourth International Conference on 3D Vision, 3DV 2016, Stanford, CA, USA, October 25-28, 2016*, pages 296–304. IEEE Computer Society, 2016. [3](#)
- [22] Yasunori Kudo, Keisuke Ogaki, Yusuke Matsui, and Yuri Odagiri. Unsupervised adversarial learning of 3d human pose from 2d joint locations. *CoRR*, abs/1803.08244, 2018. [5](#), [6](#), [7](#)

- [23] Minsik Lee, Jungchan Cho, Chong-Ho Choi, and Songhwa Oh. Procrustean normal distribution for non-rigid structure from motion. In *Proceedings of the IEEE Conference on computer vision and pattern recognition*, pages 1280–1287, 2013. 2
- [24] Matthew Loper, Naureen Mahmood, Javier Romero, Gerard Pons-Moll, and Michael J. Black. SMPL: A skinned multi-person linear model. *ACM Trans. Graphics (Proc. SIGGRAPH Asia)*, 34(6):248:1–248:16, 2015. 1
- [25] Q.-T. Luong and O.D. Faugeras. The fundamental matrix: theory, algorithms, and stability analysis. *International Journal of Computer Vision*, 17:43–75, 1995. 1
- [26] Eric Marchand, Hideaki Uchiyama, and Fabien Spindler. Pose estimation for augmented reality: a hands-on survey. *IEEE transactions on visualization and computer graphics*, 22(12):2633–2651, 2015. 1
- [27] Francesc Moreno-Noguer. 3d human pose estimation from a single image via distance matrix regression. In *Proceedings of the IEEE Conference on Computer Vision and Pattern Recognition*, pages 2823–2832, 2017. 1
- [28] David Novotny, Nikhila Ravi, Benjamin Graham, Natalia Neverova, and Andrea Vedaldi. C3dpo: Canonical 3d pose networks for non-rigid structure from motion. In *Proceedings of the IEEE International Conference on Computer Vision*, pages 7688–7697, 2019. 1, 2, 4, 5, 6, 7, 8
- [29] David Novotný, Nikhila Ravi, Benjamin Graham, Natalia Neverova, and Andrea Vedaldi. C3DPO: canonical 3d pose networks for non-rigid structure from motion. In *2019 IEEE/CVF International Conference on Computer Vision, ICCV 2019, Seoul, Korea (South), October 27 - November 2, 2019*, pages 7687–7696. IEEE, 2019. 3, 6, 7
- [30] Shaifali Parashar, Mathieu Salzmann, and Pascal Fua. Local non-rigid structure-from-motion from diffeomorphic mappings. In *2020 IEEE/CVF Conference on Computer Vision and Pattern Recognition, CVPR 2020, Seattle, WA, USA, June 13-19, 2020*, pages 2056–2064. Computer Vision Foundation / IEEE, 2020. 3
- [31] Sunghoon Park, Minsik Lee, and Nojun Kwak. Procrustean regression: A flexible alignment-based framework for non-rigid structure estimation. *IEEE Transactions on Image Processing*, 27(1):249–264, 2017. 2, 4, 7, 8
- [32] Sunghoon Park, Minsik Lee, and Nojun Kwak. Procrustean regression: A flexible alignment-based framework for non-rigid structure estimation. *IEEE Trans. Image Process.*, 27(1):249–264, 2018. 3
- [33] Sunghoon Park, Minsik Lee, and Nojun Kwak. Procrustean regression networks: Learning 3d structure of non-rigid objects from 2d annotations. In Andrea Vedaldi, Horst Bischof, Thomas Brox, and Jan-Michael Frahm, editors, *Computer Vision - ECCV 2020 - 16th European Conference, Glasgow, UK, August 23-28, 2020, Proceedings, Part XXIX*, volume 12374 of *Lecture Notes in Computer Science*, pages 1–18. Springer, 2020. 1, 2, 3, 4, 6, 7, 8
- [34] Mihir Sahasrabudhe, Zhixin Shu, Edward Bartram, Riza Alp Güler, Dimitris Samaras, and Iasonas Kokkinos. Lifting autoencoders: Unsupervised learning of a fully-disentangled 3d morphable model using deep non-rigid structure from motion. In *2019 IEEE/CVF International Conference on Computer Vision Workshops, ICCV Workshops 2019, Seoul, Korea (South), October 27-28, 2019*, pages 4054–4064. IEEE, 2019. 3
- [35] Torsten Sattler, Bastian Leibe, and Leif Kobbelt. Fast image-based localization using direct 2d-to-3d matching. In *2011 International Conference on Computer Vision*, pages 667–674. IEEE, 2011. 1
- [36] Jingnan Shi, Heng Yang, and Luca Carlone. Optimal pose and shape estimation for category-level 3d object perception. *arXiv preprint arXiv:2104.08383*, 2021. 1
- [37] Jamie Shotton, Andrew Fitzgibbon, Mat Cook, Toby Sharp, Mark Finocchio, Richard Moore, Alex Kipman, and Andrew Blake. Real-time human pose recognition in parts from single depth images. In *CVPR 2011*, pages 1297–1304. Ieee, 2011. 1
- [38] N. Snavely, S. M. Seitz, and R. Szeliski. Modeling the world from internet photo collections. *Int. J. Comput. Vision*, 80(2):189–210, 2007. 1
- [39] Carsten Steger. Algorithms for the orthographic-n-point problem. *Journal of Mathematical Imaging and Vision*, 60(2):246–266, 2018. 2
- [40] Martin Sundermeyer, Zoltan-Csaba Marton, Maximilian Durner, and Rudolph Triebel. Augmented autoencoders: Implicit 3d orientation learning for 6d object detection. *International Journal of Computer Vision*, 128(3):714–729, 2020. 1
- [41] Supasorn Suwajanakorn, Noah Snavely, Jonathan Tompson, and Mohammad Norouzi. Discovery of latent 3d keypoints via end-to-end geometric reasoning. *arXiv preprint arXiv:1807.03146*, 2018. 1
- [42] Hao Tang, Dan Xu, Gaowen Liu, Wei Wang, Nicu Sebe, and Yan Yan. Cycle in cycle generative adversarial networks for keypoint-guided image generation. In *Proceedings of the 27th ACM International Conference on Multimedia*, pages 2052–2060, 2019. 1
- [43] Lorenzo Torresani, Aaron Hertzmann, and Christoph Breger. Nonrigid structure-from-motion: Estimating shape and motion with hierarchical priors. *IEEE Trans. Pattern Anal. Mach. Intell.*, 30(5):878–892, 2008. 6, 7
- [44] Alexander Toshev and Christian Szegedy. Deeppose: Human pose estimation via deep neural networks. In *2014 IEEE Conference on Computer Vision and Pattern Recognition, CVPR 2014, Columbus, OH, USA, June 23-28, 2014*, pages 1653–1660. IEEE Computer Society, 2014. 3, 7
- [45] Shubham Tulsiani and Jitendra Malik. Viewpoints and keypoints. In *Proceedings of the IEEE Conference on Computer Vision and Pattern Recognition*, pages 1510–1519, 2015. 1
- [46] Chaoyang Wang and Simon Lucey. Paul: Procrustean autoencoder for unsupervised lifting. In *Proceedings of the IEEE/CVF Conference on Computer Vision and Pattern Recognition*, pages 434–443, 2021. 1, 2, 3, 4, 5, 6, 7, 8
- [47] Lior Wolf and Amnon Shashua. On projection matrices and their applications in computer vision. *International Journal of Computer Vision*, 48(1):53–67, 2002. 3
- [48] Shangzhe Wu, Christian Rupprecht, and Andrea Vedaldi. Unsupervised learning of probably symmetric deformable 3d

- objects from images in the wild (extended abstract). In Zhi-Hua Zhou, editor, *Proceedings of the Thirtieth International Joint Conference on Artificial Intelligence, IJCAI 2021, Virtual Event / Montreal, Canada, 19-27 August 2021*, pages 4854–4858. ijcai.org, 2021. [3](#)
- [49] Heng Yang and Luca Carlone. In perfect shape: Certifiably optimal 3d shape reconstruction from 2d landmarks. In *Proceedings of the IEEE/CVF Conference on Computer Vision and Pattern Recognition*, pages 621–630, 2020. [1](#)
- [50] Zi Jian Yew and Gim Hee Lee. 3dfeat-net: Weakly supervised local 3d features for point cloud registration. In *European Conference on Computer Vision*, pages 630–646. Springer, 2018. [1](#)
- [51] Stefanos Zafeiriou, Grigorios G Chrysos, Anastasios Rousos, Evangelos Ververas, Jiankang Deng, and George Trigeorgis. The 3d menpo facial landmark tracking challenge. In *Proceedings of the IEEE International Conference on Computer Vision Workshops*, pages 2503–2511, 2017. [1](#)
- [52] Haitian Zeng, Yuchao Dai, Xin Yu, Xiaohan Wang, and Yi Yang. Pr-rrn: Pairwise-regularized residual-recursive networks for non-rigid structure-from-motion. In *Proceedings of the IEEE/CVF International Conference on Computer Vision*, pages 5600–5609, 2021. [1](#), [2](#)
- [53] Wanqing Zhao, Shaobo Zhang, Ziyu Guan, Wei Zhao, Jinye Peng, and Jianping Fan. Learning deep network for detecting 3d object keypoints and 6d poses. In *Proceedings of the IEEE/CVF Conference on Computer Vision and Pattern Recognition*, pages 14134–14142, 2020. [1](#)
- [54] Xiaowei Zhou, Menglong Zhu, Spyridon Leonardos, Konstantinos G. Derpanis, and Kostas Daniilidis. Sparseness meets deepness: 3d human pose estimation from monocular video. In *2016 IEEE Conference on Computer Vision and Pattern Recognition, CVPR 2016, Las Vegas, NV, USA, June 27-30, 2016*, pages 4966–4975. IEEE Computer Society, 2016. [3](#)
- [55] Yingying Zhu, Dong Huang, Fernando De La Torre, and Simon Lucey. Complex non-rigid motion 3d reconstruction by union of subspaces. In *Proceedings of the IEEE conference on computer vision and pattern recognition*, pages 1542–1549, 2014. [3](#)
- [56] Yingying Zhu, Dong Huang, Fernando De la Torre, and Simon Lucey. Complex non-rigid motion 3d reconstruction by union of subspaces. In *2014 IEEE Conference on Computer Vision and Pattern Recognition, CVPR 2014, Columbus, OH, USA, June 23-28, 2014*, pages 1542–1549. IEEE Computer Society, 2014. [3](#)